Coarctation-induced degenerative abdominal aortic aneurysm in a porcine model

Pao-Yen Lin, MD,[a,b,c] Yeng-Ting Wu, MS,[d] Guan-Cheng Lin, BS,[d,e] Yao Hsiang Shih, BS,[e] Ariunaa Sampilvanjil, MD,[d] Lih-Ren Chen, PhD,[f] Yu-Jen Yang, MD, PhD,[c] Hua-Lin Wu, PhD,[b,g] and Meei Jyh Jiang, PhD,[b,d] *Tainan, Taiwan*

Objective: **Hemodynamic stress participates in the initiation and progression of aneurysmal degeneration. Coarctation increases flow-mediated stress on the aortic wall. We tested the hypothesis that prolonged coarctation of an infrarenal abdominal aorta (AA) segment leads to abdominal aortic aneurysm (AAA) formation in mini pigs.**

Methods: **An asymmetric, funnel-shaped flow path was created by constricting the infrarenal AA segment of Taiwanese Lanyu mini pigs (age, 7-10 months; male and female) wrapped with an 8-mm-wide expanded polytetrafluoroethylene Teflon strip for 4 weeks (4w), 8 weeks (8w), and 12 weeks (12w) (seven pigs per group). This mimics the tortuous aneurysm neck in human AAA, which increases downstream flow-mediated stress. Significant flow disturbance resulting from moderate coarctation was indicated by a pulsatility index reduced to one third the inherent levels. Sham control pigs received Teflon wrapping without coarctation.**

Results: **Aneurysm characterized by progressive medial degeneration occurred at the terminal AA after 12w coarctation. The outer dimension enlargement of the distal AA exceeded 50% compared with that of the proximal AA at 4w, 8w, and 12w postcoarctation (sham, 1.0; 4w, 1.7 ± 0.08; 8w, 1.5 ± 0.09; 12w, 1.7 ± 0.01). Lumen ratio of the distal-to-suprarenal AA increased time dependently, with 12w postcoarctation exhibiting significant increase (sham, 1.0 ± 0.05; 4w, 1.1 ± 0.11; 8w, 1.4 ± 0.20; 12w, 1.5 ± 0.09). In the distal AA, elastic lamellae exhibited fragmentation at 4w and more pronounced fragmentation with decreased density at 8w and 12w postcoarctation. Medial collagen density exhibited the trend to increase at 4w and 8w but was reversed at 12w postcoarctation. Smooth muscle exhibited disarray and nuclear density decrease at 8w and 12w postcoarctation (sham, 6966 ± 888/mm^2; 4w, 5747 ± 1340/mm^2; 8w, 4153 ± 323/mm^2; 12w, 4083 ± 465/mm^2). Gelatin zymography revealed that matrix metalloproteinase-9 activity markedly increased at 4w postcoarctation.**

Conclusions: **Prolonged moderate coarctation caused regional hemodynamic stress and thereby induced degenerative AAA in the terminal AA. (J Vasc Surg 2013;57:806-15.)**

Clinical Relevance: **The present study demonstrates that persistent hemodynamic stress participates in the progression of aneurysmal degeneration. Moderate coarctation not only increases regional hemodynamic stress on the terminal aorta but also creates an asymmetric and angulated inflow tract similar to the tortuous aneurysm neck. Restoring normal flow pattern in the aneurysm sac as well as reducing regional hemodynamic stress by correcting the tortuous neck may prevent or reverse further aneurysmal degeneration. This porcine abdominal aortic aneurysm model provides a versatile platform to investigate abdominal aortic aneurysm pathogenesis and to develop new therapeutics.**

Abdominal aortic aneurysm (AAA) is a common and life-threatening disease that affects 4% to 8% of the population older than 65 years.[1] The disease process is mainly localized at the infrarenal abdominal aortic (AA) segment, where gradual weakening and dilatation of the aortic wall develop as consequences of chronic structural degeneration.[2] Most AAAs remain asymptomatic until the catastrophic event of rupture occurs. However, the risk of death exceeds 80% once aneurysm ruptures.[3] The current strategy for AAA treatment focuses on preventing aneurysm rupture. In spite of the improvement in diagnostic imaging modalities and surgical techniques with less invasive endovascular aneurysm repair, no significant progress has been made toward improving the morbidity and mortality of AAA at such an advanced stage.[4,5] Therefore, changing the strategy from passively preventing late rupture to actively reducing early degeneration should provide an avenue for improving outcomes of AAA treatment.[6,7]

Reducing aneurysmal degeneration relies on thoroughly understanding the pathogenesis of AAA. Along the area of AAA degeneration, the aneurysmal wall is characterized by progressive destruction of extracellular matrix (ECM). Destruction of ECM results from two highly connected processes, consecutive inflammatory responses and excessive

From the Institute of Clinical Medicine,[a] the Cardiovascular Research Center,[b] the Department of Cell Biology and Anatomy,[d] the Institute of Basic Medical Sciences,[e] and the Department of Biochemistry and Molecular Biology,[g] National Cheng Kung University College of Medicine; the Department of Surgery, Division of Cardiovascular Surgery, National Cheng Kung University Hospital[c]; and the Taiwan Livestock Research Institute.[f]

This work was supported by the National Science Council (NSC95-2752-B-006-003-PAE, NSC98-2320-B-006-025-MY3) and NCKU Hospital (NCKUH-9803025, -9903053, -10003023) of Taiwan.

Author conflict of interest: none.

Additional material for this article may be found online at www.jvascsurg.org.

Reprint requests: Meei Jyh Jiang, PhD, Department of Cell Biology and Anatomy, College of Medicine, National Cheng Kung University, 1 Ta-Hsueh Road, Tainan 70101, Taiwan (e-mail: mjiang@mail.ncku.edu.tw).

The editors and reviewers of this article have no relevant financial relationships to disclose per the JVS policy that requires reviewers to decline review of any manuscript for which they may have a conflict of interest.

0741-5214/$36.00

http://dx.doi.org/10.1016/j.jvs.2012.08.104

proteolytic degradation, which lead to decreased tensile strength and increased wall tension. When wall stress exceeds tensile strength, aneurysm rupture occurs.[8] However, compelling evidence reveals that aneurysmal degeneration is not a uniform and irretrievable process. Instead, the process represents a seesaw contest between repair and destruction of vascular ECM up to the rupture stage.[9] Therefore, identifying the pathophysiologic factors that harness degeneration or facilitate destruction of the vessel wall should help in the development of new diagnostic and therapeutic modalities for AAA.

To gain insight into the pathogenesis of AAA development, an animal model mimicking early human aneurysmal degeneration is needed. Using chemical or surgical means, various animal models have been developed to mimic AAA in humans.[10] However, discrepancies exist between experimentally induced AAAs and degenerative aneurysm in humans; in particular, the earliest inciting process remains elusive.[10] Mini pigs have a physical size suitable for surgical manipulation. Moreover, the cardiovascular system of pig, both anatomically and physiologically, is almost the same as that of human.[11] Therefore, we attempted to simulate aneurysmal degeneration by modeling the porcine aorta with coarctation. Coarctation increases hemodynamic stress on the aortic wall and creates flow disturbance. Previous studies showed that hemodynamic stress is relevant to AAA predisposition and that flow variability markedly influences arterial lumen diameter.[12-15] A recent study applied a perivascular cast to modify shear stress of the carotid artery in apolipoprotein E $(ApoE)^{-/-}$ mice and showed that both lower and oscillatory shear stresses induce atherosclerosis.[16] Interestingly, poststenotic arterial dilatation was detected at the area exhibiting oscillatory shear stress distal to the cast.[16] We hypothesized that prolonged coarctation at the infrarenal AA segment induces outward vascular remodeling and consequently leads to AAA formation. Using an expanded polytetrafluoroethylene (ePTFE) strip to perform a funnel-shape coarctation in an infrarenal AA segment of mini pigs, we detected 50% luminal dilatation in the distal AA segment at 12 weeks postcoarctation. Macroscopic and microscopic results indicated that we successfully established a coarctation-induced degenerative AAA model in swine.

METHODS

Animals. Experimental animals used in this study were Taiwanese Lanyu mini pigs, which have been qualified as an excellent pig strain for cardiovascular research.[17] Further information on Taiwanese Lanyu pigs can be found on the website http://minipigs.angrin.tlri.gov.tw. All experimental pigs (7- to -10-month-old adults; both genders) were provided by Taitung Animal Propagation Station of the Taiwan Livestock Research Institute and completed the quarantine before experiments. Thirty mini pigs were randomly divided into six groups: three experimental groups (seven pigs per group) undergoing aortic coarctation for 4 weeks (4w), 8 weeks (8w), and 12 weeks (12w) and three sham groups (4w, 8w, and 12w; three pigs per group) as the control. The whole study conforms to the *Guide for the Care and Use of Laboratory Animals* published by the National Institutes of Health, and the experimental procedures were approved by the institutional Animal Care and Use Committee.

Anesthesia and aortic coarctation. Preanesthesia induction of mini pigs was conducted by intramuscularly injecting a mixture of tranquilizer, analgesics, and anticholinergics containing a mixture of zolazepam and tiletamine (10 mL), xylazine hydrochloride (5 mL), and atropine (1 mL) at the pigs' posterior neck or gluteal region. The sedated pigs were placed on the operation table in the supine position, and intravenous fluid infusion routes were established through the postauricular veins. Endotracheal intubation was performed, and isoflurane (2% of tidal volume) was continuously given during surgery to maintain general anesthesia. To better expose the infrarenal aorta and bilateral common iliac arteries, a transperitoneal cavity approach via laparotomy was taken. After the retroperitoneum was opened, infrarenal AA was isolated free from the surrounding tissues. An ePTFE Teflon strip with 8-mm-diameter to simulate the infrarenal AA size was used to encircle the AA approximately 2 cm above the bifurcation of aorta. We have found that coarctation at this location consistently generates flow turbulence and induces aneurysm. The Teflon strip was tailored to a funnel-shaped tube that modeled the wrapped aortic segment into a tapered channel with a nonconstrictive inlet and a constrictive outlet (Fig 1, *A*). The sham group underwent a retroperitoneal opening, AA isolation, and Teflon strip wrapping without aortic coarctation. The surgical procedure was carried out under aseptic conditions and was completed within 3 hours to avoid respiratory distress caused by prolonged supine posture.

Quantitative characterization of aortic coarctation. Aortic coarctation may create resistive hemodynamic conditions (ie, diminished anterograde flow and oscillatory shear stress) that mediate aneurysm formation.[18] However, neither very tight nor mild luminal constriction produces marked flow disturbance.[19] The excellent resilience of the aortic wall against cyclic deformation usually prevents the inner lumen from stenosing upon external compression. Moreover, the susceptibility to vasospasm along the pulsating wall often makes accurate measurement of the luminal diameter of aorta difficult. To achieve moderate coarctation, we chose the pulsatility index to quantitatively characterize hemodynamic changes. The pulsatility index was calculated by dividing the difference between the maximal and minimal flow rate by the mean flow rate. [20,21] The reduction of the pulsatility index is proportional to the severity of aortic coarctation.[22,23] Hence, our criteria for moderate coarctation were pulsatility index reduction to one third of the inherent level (Fig 1, *B*) combined with turbulent flow in the aortic segment distal to the constriction (Fig 2). A transit time flowmeter system (MediStim VeriQ system; MediStim ASA, Oslo, Norway) was used during the operation to simultaneously monitor flow, pressure, and pulsatility index changes at the regions

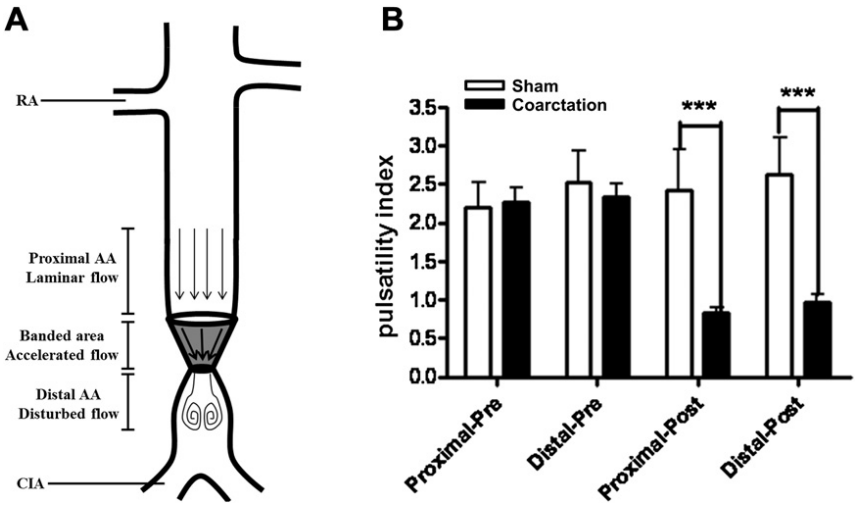

Fig 1. Coarctation decreased pulsatility index in both proximal and distal abdominal aorta (*AA*) segments. **A,** Location of coarctation at an infrarenal AA segment approximately 2 cm proximal to the iliac bifurcation. An 8-mm-long expanded polytetrafluoroethylene strip was used to encircle the infrarenal AA segment with a nonconstrictive inlet and a constrictive outlet. **B,** Transit time flowmeter system used during operation to simultaneously monitor changes in flow, pressure, and pulsatility index at regions proximal and distal to the coarctation. Values were expressed as mean ± standard error of the mean (sham, n = 4; coarctation: n = 8). *CIA*, Common iliac artery; *RA*, renal artery. ***$P < .005$ vs sham group.

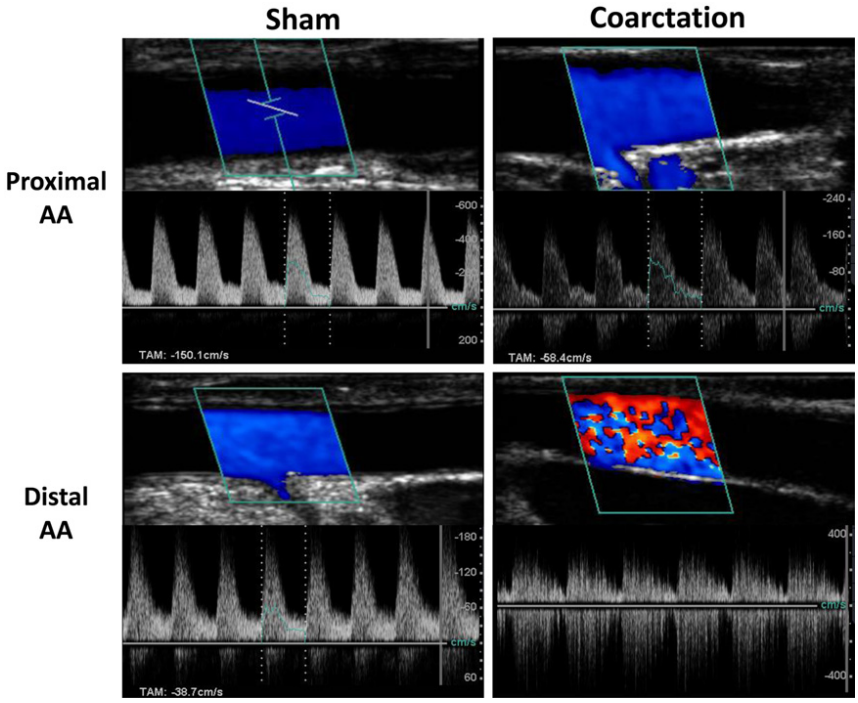

Fig 2. Coarctation-induced turbulent flow in the distal abdominal aorta (*AA*) segment. Duplex ultrasound scanning was conducted during the coarctation procedure to monitor flow patterns in both proximal and distal AA segments. Ultrasound scanning images showed a mosaic flow pattern in the distal AA segment after coarctation and a lamellar flow pattern in the proximal AA segment and sham control. Doppler spectral analysis indicated decreased peak systolic flow and increased reverse flow after coarctation, whereas sham operation had little effect on flow pattern.

proximal and distal to the coarctation. Flow turbulence was detected by duplex ultrasound scanning (MicroMaxx; SonoSite, Bothell, Wash), which provides a mosaic color pattern of flow and Doppler spectral analysis that shows simultaneous forward and reverse flow, spectrum fill-in, and ill-defined spectrum margins after coarctation.

Sacrifice and tissue collection/processing. Mini pigs were anesthetized as described for the coarctation operation. Before the retroperitoneum was opened, duplex ultrasound scanning was performed to acquire images of the aortic lumen at the distal AA segment. After the infrarenal AA was isolated, blood flow, pulsatility index (PI), and intraluminal blood pressure at the proximal and distal AA segments were monitored. In addition, the outer diameter of various AA segments was measured. Animals were then sacrificed with an intravenous injection of KCl (2 mmol per kilogram body weight). The AA segments from regions proximal and distal to the coarctation and the suprarenal area were collected. Tissues were fixed in 4% buffered paraformaldehyde, dehydrated with sequential incubation with ethanol from 70% to 100%, cleared with xylene, and embedded with paraffin.

Histologic examination of the abdominal aorta. To examine the overall morphology and the distribution of elastic lamellae and collagen fibers in various AA segments, hematoxylin-eosin, Verhoeff-van Gieson, and Masson trichrome staining was performed. Paraffin sections (4 μm thick) were deparaffinized, rehydrated, and stained according to the manufacturer's instructions.

Detecting smooth muscle density with immunohistochemistry. Paraffin sections of different AA segments were processed and incubated overnight with monoclonal antibody against smooth muscle-specific α-actin (1:400, clone 1A4; Sigma, St. Louis, Mo; or clone E184; Epitomics, Burlingame, Calif) at 4°C. To detect the assembly of medial vascular smooth muscle cells (VSMC), aortic sections were subsequently incubated with horseradish peroxidase-conjugated horse antimouse immunoglobulin and chromogen substrate and counterstained with hematoxylin. To examine the number of nuclei in the medial VSMC, aortic sections were subsequently incubated with Alexa 594-conjugated horse antimouse immunoglobulin and Hoechst 33342.

Quantification. Aortic lumen perimeter, medial smooth muscle percent area, and medial nuclear density were measured by Image Pro-Plus (Media Cybernetics, Rockville, Md). The relative abundance of collagen and elastic fibers in the media was quantified as previously described in four sections with 80-μm intervals and four fields (100× magnification) each.[24]

Gelatin zymography. Gelatin zymography was performed according to Davis et al[25] (see the Appendix, online only, for details.)

Statistical analysis. Data are expressed as mean ± standard error of the mean; n is the number of pigs. Data were analyzed first with one-way analysis of variance, followed by Tukey honestly significant difference test between groups. Statistical significance was set at $P < .05$.

RESULTS

Changes in blood pressure and pulsatility index. We measured blood pressure at the AA segments proximal and distal to the coarctation site after operation and before sacrifice in 12 pigs. Following coarctation, systolic blood pressure at the distal AA decreased and a pressure gradient of approximately 30 mm Hg was detected between the proximal and distal AA segments. In contrast, diastolic blood pressure did not vary between these AA segments. Interestingly, systolic blood pressure at the distal AA had returned to pre-operation levels at sacrifice (Table). Similarly, PI values had reversed to preoperation levels similar to those of sham control (coarctation group: proximal AA, 2.7 ± 0.33; distal AA, 2.7 ± 0.35, n = 12; sham group: proximal AA, 2.4 ± 0.55, distal AA, 2.4 ± 0.56, n = 5).

Table. Systolic and diastolic blood pressure levels in AA segments proximal and distal to coarctation at operation and sacrifice

	Proximal AA		*Distal AA*	
	Sham, mm Hg	*Coarctation, mm Hg*	*Sham, mm Hg*	*Coarctation, mm Hg*
Operation				
SBP	99 ± 10.0 n = 4	98 ± 3.8 n = 8	93 ± 10.5 n = 4	65 ± 9.9[a] n = 8
DBP	68 ± 11.8 n = 4	64 ± 4.4 n = 8	67 ± 11.4 n = 4	53 ± 5.6 n = 8
Sacrifice				
SBP	98 ± 6.8 n = 3	89 ± 3.5 n = 8	98 ± 7.5 n = 3	94 ± 4.9 n = 8
DBP	67 ± 9.4 n = 3	61 ± 2.4 n = 8	68 ± 9.5 n = 3	61 ± 2.4 n = 8

AA, Abdominal aorta; *DBP,* diastolic blood pressure; *SBP,* systolic blood pressure.
Values are given as mean ± standard error of the mean. SBP and DBP were measured intraluminally using the MediStim VeriQ system.
[a]$P < .01$ vs sham group.

Coarctation-induced AAA formation in mini pigs. To determine whether coarctation induced aneurysm, we examined both the luminal and the outer diameters of the infrarenal AA segments before sacrifice and measured the luminal perimeters of the distal AA segments in cross sections. The luminal diameters of both proximal and distal AA segments were examined with duplex ultrasound scanning after the retroperitoneum was opened. The lumen of the distal AA segment at 12w postcoarctation exhibited pronounced dilatation whereas that of the sham group was near constant in size (Fig 3, *A*). The outer diameter of the distal AA segment markedly increased at 4w postcoarctation and remained a similar size up to 12w postcoarctation (Fig 3, *B*). In the infrarenal aorta with length of 5.8 ± 0.31 cm (n = 10), the isolated AAA appeared fusiform, was located at the distal segment, and often extended to the common iliac arteries. Because the proximal AA segment often exhibited pronounced intimal thickening that rendered lumen measurement less accurate, we used the suprarenal AA as the reference. Hematoxylin-eosin staining showed that the lumen perimeter ratio of the distal-to-suprarenal segment increased at 8w postcoarctation and reached approximately 50% at 12w postcoarctation (8w, 1.4 ± 0.20, n = 6; 12w, 1.5 ± 0.09, n = 7; sham, 1.0 ± 0.05, n = 9). In contrast, the lumen

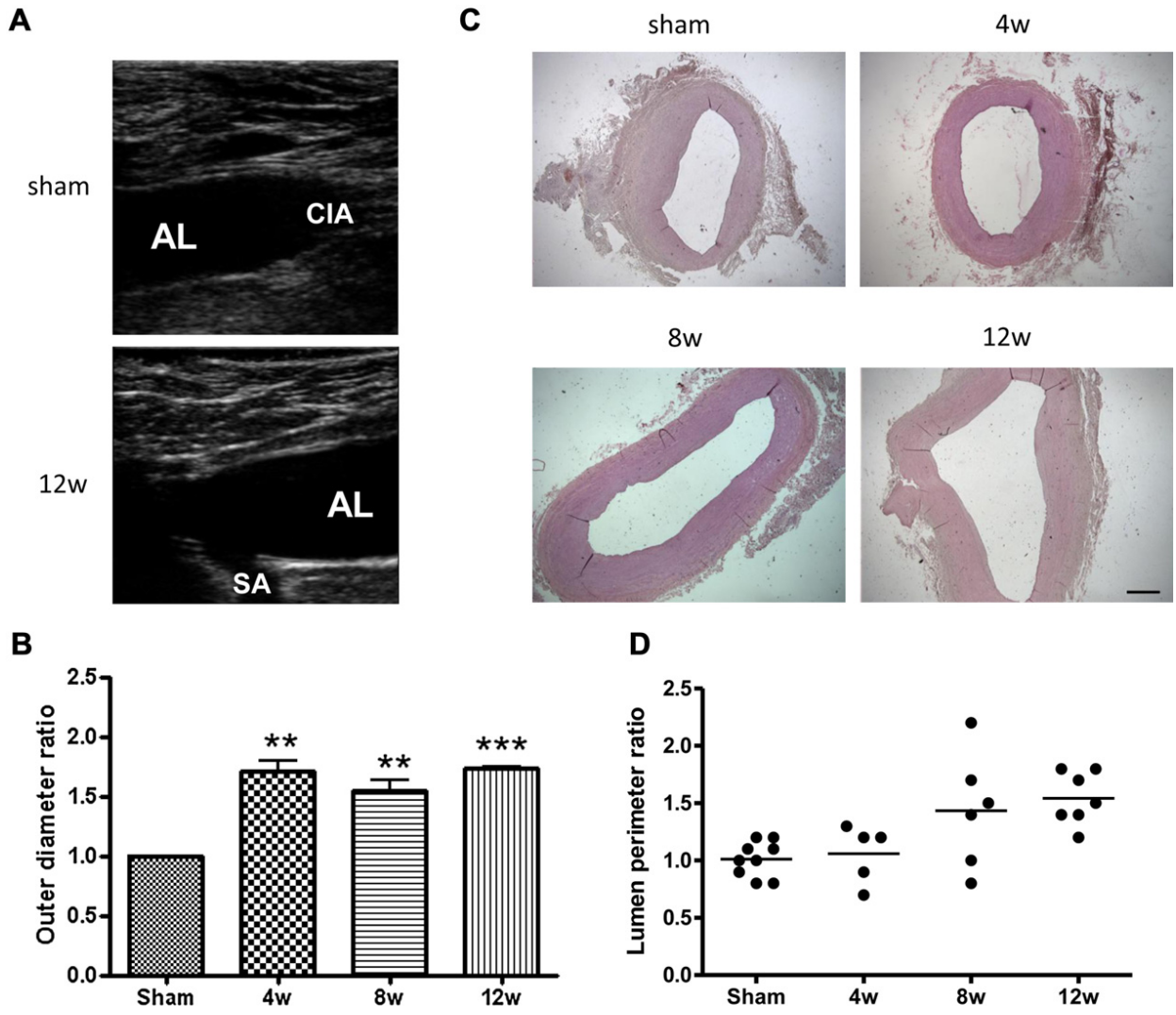

Fig 3. Outer diameter and lumen perimeter of the distal abdominal aorta (AA) segment increased after coarctation. **A,** Representative duplex ultrasound scanning images showing increased lumen size in the distal AA segment at 12 weeks (*12w*) postcoarctation before sacrifice and uniform lumen in the sham group. **B,** Outer diameter of proximal and distal AA segments was measured after isolation of AA in the retroperitoneum. The ratio of distal-to-proximal AA diameter was calculated. $^{**}P < .01$, $^{***}P < .001$ vs sham group. **C** and **D,** Hematoxylin-eosin staining of the distal AA segment (cross section) from sham group and experimental group at 4 weeks (*4w*), 8 weeks (*8w*), and 12 weeks (*12w*) postcoarctation. **C,** Representative results. *Scale bar*: 1000 μm. **D,** Lumen perimeter ratio of distal-to-suprarenal AA segment. Lumen perimeter ratio at 12w postcoarctation increased compared with sham group ($P < .05$). *AL,* Aortic lumen; *CIA,* common iliac artery; *SA,* spinal artery.

perimeter of the distal AA segment at 4w postcoarctation did not change compared with that of the sham control (1.1 ± 0.11, n = 5; Fig 3, *C* and *D*).

Changes in elastic lamellae and collagen fibers during AAA formation. To characterize the structural changes in the AA wall, we examined the density of elastic lamella with Verhoeff staining. In the distal AA at 4w postcoarctation, the density of elastic lamellae in the media did not change, but fragmentation was easily detected compared with sham control. The decrease and fragmentation of elastic lamellae were more pronounced at 8w and 12w postcoarctation (Fig 4, *A* and *B*). Interestingly, elastic fibers in the adventitia appeared to increase at 4w and 8w postcoarctation but returned to basal levels at 12w postcoarctation.

We next examined the distribution of collagen fibers in the AA segments. Collagen fibers were mainly distributed in the adventitia, with a lower density in the media of the sham group (Fig 4, *C* and *D*). The density of collagen fibers in the media of the distal AA segment exhibited a trend to increase at 4w and 8w postcoarctation but returned to basal levels at 12w postcoarctation. In addition, prominent collagen fibers were detected in focally thickened intima at both 8w and 12w postcoarctation.

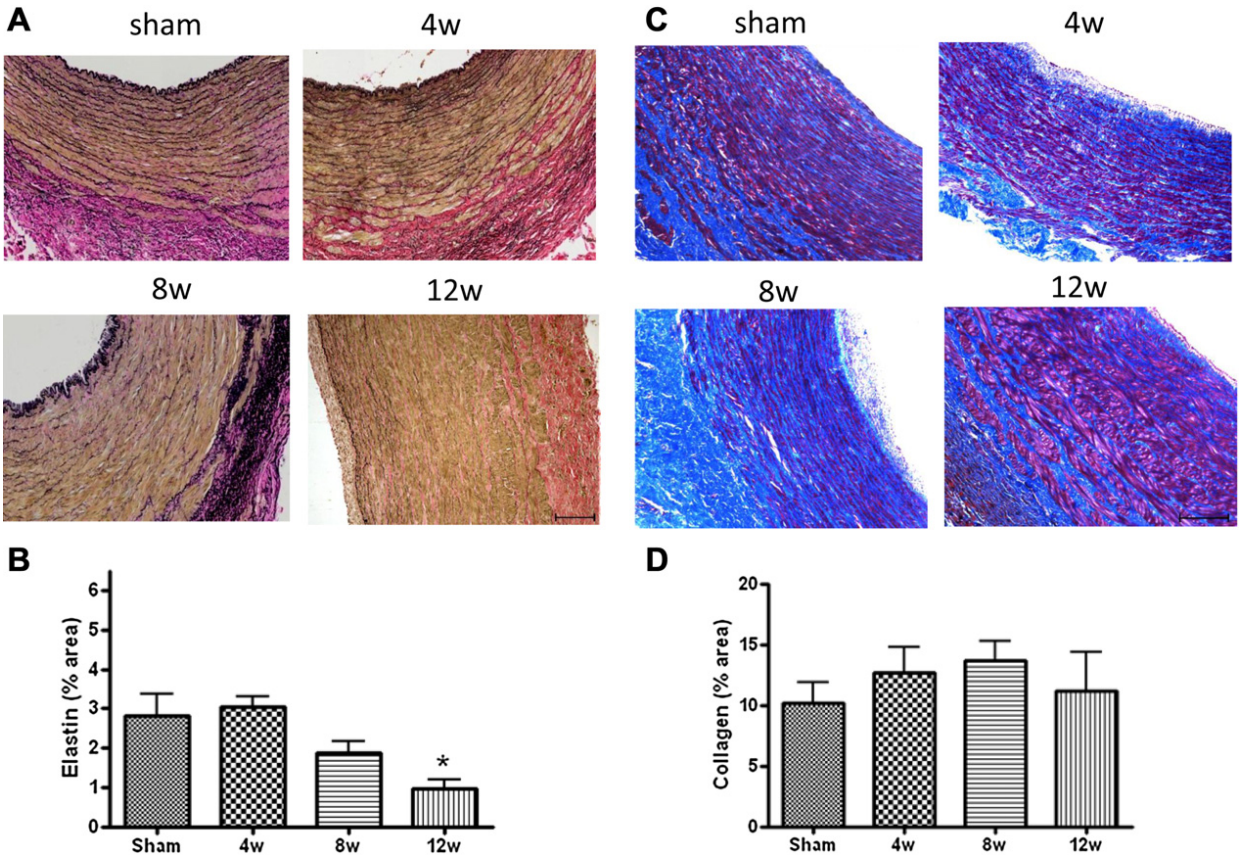

Fig 4. Changes in elastic lamella and collagen fibers in coarctation-induced abdominal aortic aneurysm (AAA). Elastic fibers **(A** and **B)** and collagen fibers **(C** and **D)** in the distal AA segment (cross section) from the sham group and experimental groups of 4 weeks (*4w*), 8 weeks (*8w*), and 12 weeks (*12w*) postcoarctation were examined. Elastic fibers were examined with Verhoeff-van Gieson staining. Collagen fibers were examined with Masson trichrome staining. **A** and **C,** Representative results. *Scale bar*: 200 μm. **B** and **D,** Relative abundance of elastic lamella **(B)** and collagen fibers **(D)**. Values are given as mean ± standard error of the mean (**B,** n = 4∼8; **D,** n = 3∼4). **P* < .05 vs sham.

Smooth muscle cell density decreased during AAA formation. To examine whether changes occurred in smooth muscle cells during AAA formation, we stained distal AA sections with smooth muscle-specific α-actin and counted nuclear density in the media. No significant change in percent area of VSMC was detected (Fig 5, *b*). In contrast, the nuclear density of the media decreased markedly at 8w and 12w postcoarctation (Fig 5, *c*). These results suggest that VSMC hypertrophy occurred during AAA progression. Interestingly, in the distal AA, alignment of VSMC near the adventitia appeared to change from circularly oriented, highly ordered layers to longitudinally oriented bundles in some areas of the media both at 8w (Fig 5, *a, c,* and *e*) and 12w (Fig 5, *a, d,* and *f*) postcoarctation. In some areas of the distal AA sections, the boundary between media and adventitia was difficult to define.

Metalloproteinase activity increased during AAA formation. Because matrix metalloproteinase (MMP)-2 and MMP-9 play important roles in AAA formation, we examined their activity in the distal AA segment using gelatin zymography. The MMP-2 exhibited high intrinsic activity that did not increase after coarctation. In contrast, proMMP-9 activity exhibited a trend to be higher in the coarctation groups compared with the sham control and was significantly upregulated at 4w postcoarctation (Fig 6).

DISCUSSION

Our results clearly showed that prolonged coarctation for 12w induces infrarenal AAA at the distal AA segment. The maximal outer dimension of aneurysm usually was >1.5-fold that of the segment proximal to coarctation. Histologic examination detected enlargement of the lumen at the distal AA after prolonged coarctation. The distal-to-suprarenal AA luminal perimeter ratio indicated lumen dilatation of the distal AA at 8w and 12w postcoarctation. Moreover, the ratio increased with the period of coarctation, suggesting that longer coarctation leads to further aneurysm expansion. Although 4w coarctation did not lead to lumen enlargement, structural degeneration that nevertheless developed during this period as fragmentation of elastic lamellae was easily detected in the aortic media. Destruction of elastic lamellae became pronounced in the aneurysmal walls at 8w and 12w postcoarctation, with

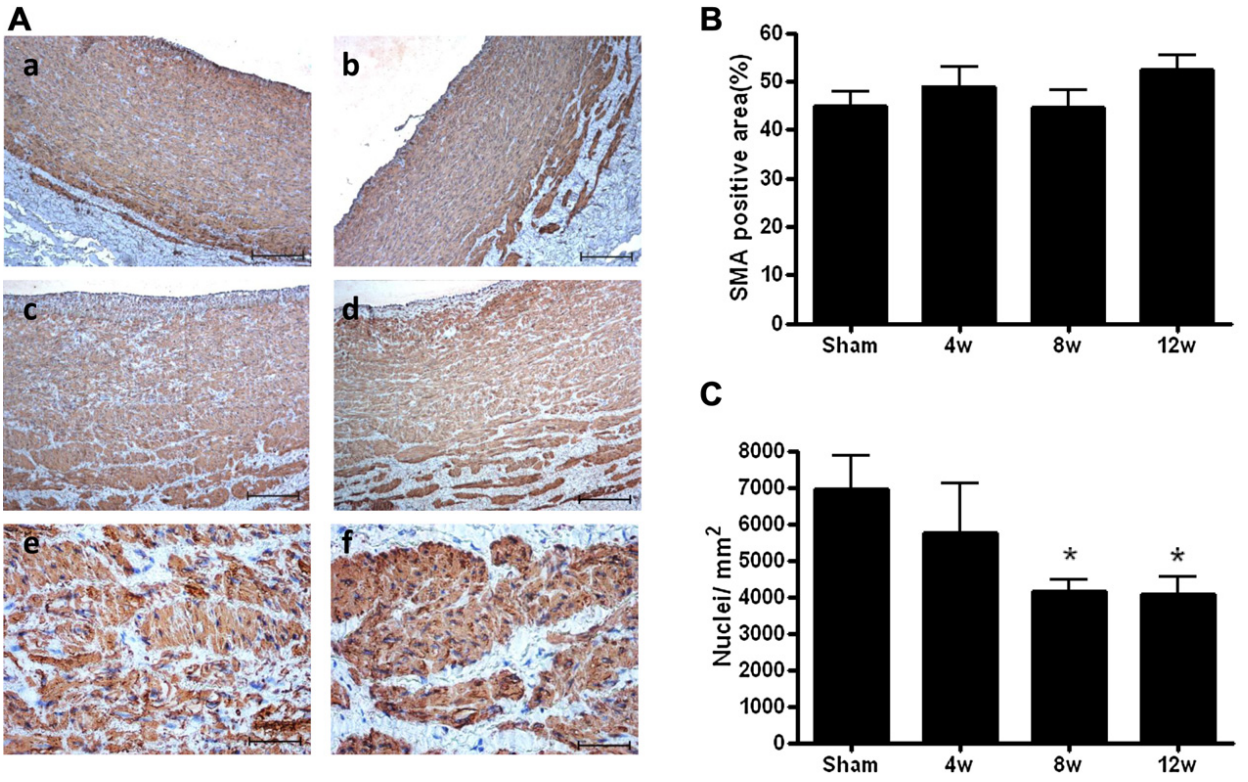

Fig 5. Smooth muscle cell density decreased during abdominal aortic aneurysm (AAA) formation. **A** and **B,** Smooth muscle abundance in the distal abdominal aorta (AA) segment of sham group **(a)** and experimental groups of 4 weeks (*4w*; **b**), 8 weeks (*8w*; **c** and **e**), and 12 weeks (*12w*; **d** and **f**) postcoarctation was assessed with smooth muscle-specific α-actin (SMA)-positive area. **A,** Representative results. *Scale bars*: 200 μm **(a-d);** 50 μm **(e** and **f). B,** The SMA-positive area is presented as mean ± standard error of the mean (n = 3∼6). **C,** Cross sections of the distal AA segment from various groups stained with SMA immunofluorescence and Hoechst 33342. Smooth muscle cell nuclei were counted in the media and nuclear density presented as mean ± standard error of the mean (n = 4∼8).

severe loss detected at 12w postcoarctation (Fig 4). Progressive loss of elastic lamellae in the AAA segment was accompanied by lower elasticity in 50% of pigs at 4w postcoarctation, lower elasticity at 8w, and lost elasticity at 12w of the banded aortic segment when the Teflon strip was removed. Taken together, these results strongly suggest that prolonged coarctation for 12w induces degenerative AAA.

Changes of medial collagen density also characterize the degeneration processes in coarctation-induced AAA. At 4w and 8w postcoarctation, medial collagen density exhibited a trend to increase, which may represent a mechanism to compensate for elastic lamellae degradation in earlier stages of aneurysm progression. In accordance, loss of medial collagen upregulation at 12w postcoarctation may indicate decompensation of collagen homeostasis.[9] Longer coarctation may result in prevailing collagen degradation, which attenuated the tensile strength of the aortic wall and, combined with profound elastic lamella degradation, conferred advanced medial degeneration and led to aneurysmal dilatation. It is noteworthy that gelatinolytic activity of MMP-9 was higher at 4w and 8w postcoarctation than at 12w postcoarctation, whereas no change was detected for MMP-2. These results are in discrepancy with previous studies reporting increased MMP-2 activity in human AAA spacemens.[25] The discrepancy could reflect differences between early- and late-stage AAA and is consistent with the involvement of other factors in addition to hemodynamic stress in late-stage human AAA. To clarify the roles of MMPs in ECM degradation during AAA progression, further studies examining changes in tissue inhibitors of metalloproteinases and the activity ratios between MMPs and tissue inhibitors of metalloproteinases are warranted.

In our coarctation-induced AAA model, VSMC nuclear density significantly decreased at 8w and 12w postcoarctation, whereas the percent area of VSMC did not change as assessed with smooth muscle-specific α-actin expression. The decrease in VSMC density, approximately 40%, exhibited features similar to, but less pronounced than, that reported in large human AAAs (>4.5 cm).[26] This feature suggests that AAA at 12w postcoarctation probably is at an earlier stage than large human AAAs. The decreased cell density in combination with relatively constant cell area suggests that smooth muscle cell hypertrophy occurs during coarctation-induced AAA progression. During aneurysm development, we detected disordered

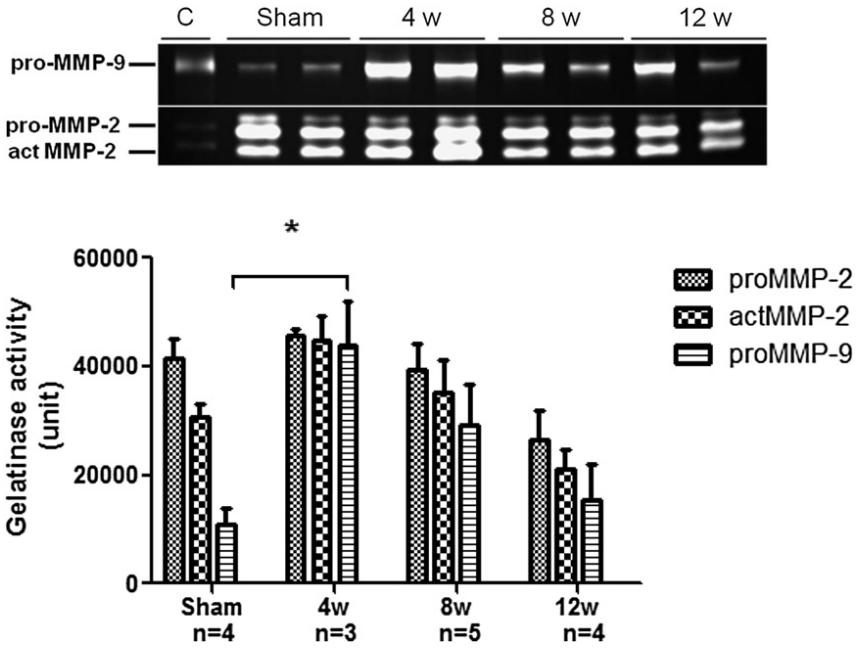

Fig 6. Matrix metalloproteinase (*MMP*)-9 activity increased during abdominal aortic aneurysm (AAA) formation. Activity of MMP-2 and MMP-9 was assessed by gelatin zymography in the distal AA segment of the control group and the coarctation groups at 4 weeks (*4w*), 8 weeks (*8w*), and 12 weeks (*12w*) postcoarctation. Tissue homogenates (30 μg of protein) were separated with sodium dodecyl sulfate-polyacrylamide gel electrophoresis containing gelatin, renatured, and incubated. Enzyme activity was detected as clear bands following Coomassie blue staining and destaining. **A,** Representative results. **B,** Quantitative results expressed as mean ± standard error of the mean ($n = 3 \sim 5$). $^*P < .05$ vs sham.

assembly of VSMC, which became more pronounced as aneurysmal dilatation progressed between 4w and 12w postcoarctation (Fig 5). In these regions of aneurysmal wall, the orderly and circular array of alternating VSMC layers and elastic lamella was replaced with disarrayed VSMC and fragmented, or even scarce, elastic lamellae. This phenomenon correlates well with our results showing that MMP-9 gelatinolytic activity increased in the distal AA during AAA development (Fig 6). Intriguingly, VSMC disorganization did not occur in the whole aneurysmal wall but instead appeared in multiple discrete regions. The uneven distribution of VSMC disarray likely results from the disparity of hemodynamic stresses, which were shown to modulate the expansion rate of elastase infusion-induced AAA in a rat model.[27] In the outer media near the adventitia, VSMC bundles, which replaced regular cell layers, became more pronounced and were surrounded with collagen fibers as the coarctation period increased. The concomitant loss of discrete elastic lamellae and VSMC layers rendered the boundary between media and adventitia difficult to define. It is interesting to note that deficiency in key regulatory proteins for VSMC-ECM interaction, such as fibulin-4 and integrin-linked kinase, leads to aneurysm in the thoracic aorta.[28,29] Whether VSMC remodeling varies as AAA progresses into different stages remains to be examined.

Our results indicated that both at initiation and during progression of AAA, hemodynamic forces participate in the evolutionary degeneration process. Three hemodynamic forces are recognized to be relevant to AAA pathogenesis: wall shear stress, tensile stress, and hydrostatic pressure.[30] Pulsatile blood flow transmits kinetic energies on aortic tissues with different orientation and hence generates the aforementioned hemodynamic forces.[31] When flow is disturbed, fluctuation of hemodynamic forces induces a variety of pathophysiologic responses that destroy the structural integrity of the aortic wall.[18,32] By constricting an infrarenal AA segment, we created a disturbed flow environment at the distal region where oscillatory shear stress was pronounced. Consequently, AAA developed and aneurysmal degeneration continued to evolve under the persistent impact of regional pathologic hemodynamics. It is noteworthy that the adjacent position of the coarctation site to the aortic bifurcation, approximately 2 cm apart, appeared to facilitate aneurysm formation. This may result from more pronounced flow disturbance that is consistent with the low oscillatory shear stress and increased pulse wave reflection/wall strain detected near the aortic bifurcation, which increase aneurysm susceptibility of the site.[15,33]

Our experimental model also suggested that moderate restriction and distortion of an aortic segment predispose distal AA to aneurysmal degeneration. Aortic coarctation not only disturbs the forward laminar flow but also interrupts the normal cyclic strain of aorta. As a result, turbulent flow in concert with limited pulsation entangles the distal

AA with resistive hemodynamics that facilitates AAA formation.[18] However, a standard parameter for quantifying moderate coarctation has never been established. Palpable thrill or audible bruit, which has been used as the criterion for significant peripheral arterial stenosis, is highly subjective and fails to consistently assess the severity of aortic coarctation.[19,34] Everlasting pulsation, keen vasospastic reaction, and excellent resilience capability interfere with precise measurement of aortic diameter. On the other hand, changes of flow rate should reflect the genuine magnitude of constriction because a decrease in peak systolic flow rate is proportional to an increase in aortic coarctation. Pulsatility index provides an objective index of the extent of coarctation and is not readily affected by physiologic activities of the aorta.[22] Therefore, we chose the pulsatility index as the quantitative parameter of coarctation in our experiments. Our results showed that 65% reduction of the original pulsatility index produced pronounced turbulence in the downstream AA region where mosaic turbulent flow was detected by color Doppler images and disturbed spectral pattern was shown by Doppler spectral analysis (Fig 2). Thus, we defined pulsatility index reduction to one third of the inherent level as the optimal degree of constriction. By constricting the aortic lumen in light of pulsatility index change, aneurysmal degeneration invariably developed in our experimental groups.

Finally, moderate coarctation can transform the local AA into an angled or distorted curve flow path, which downstream will produce an asymmetric velocity profile. Biomechanical ex vivo studies revealed that flow asymmetry may affect the distribution of wall stress and induce secondary flow and subsequently influence wall remodeling of AAA.[35] Our experimental findings, such as uneven distribution of VSMC disarray and focal intimal thickening in aneurysmal walls, provided in vivo evidence supporting these postulations. In addition, we applied a compliant ePTFE band to conduct aortic coarctation; consequently, the modeled inlet was an asymmetric inflow channel instead of a stenotic entrance as reported previously.[16] As observed by duplex ultrasound scanning, it was surprising to note that immediately after coarctation, the lumen diameter of the constrictive AA region was highly variable and in some cases decreased little compared with that of the nonconstrictive AA region, even with 65% reduction of PI (Fig 2). Based on this result, we propose that the severity of downstream AA pathology is determined mainly by the effect of coarctation on the flow profile instead of lumen size. Meanwhile, asymmetric inflow channel simulating angulated AAA necks commonly encountered in the clinical setting also is consistent with this model.

CONCLUSIONS

Sustained moderate coarctation for 12w caused regional hemodynamic stress on the terminal AA and induced genuine degenerative AAA in swine. This large animal model of AAA provides a platform for both pathogenesis investigations and translational research.

We thank Ms Chou-Hwei Lee, Mr Chi-Chung Ko, and Mr Zhi-jie Tsao for excellent surgical assistance; Mr Lin-Hsiang Yeh and Ms I-Ching Tsai for assisting with data analysis; Dr Jin-Jia Hu for providing the histologic staining quantification method; and Prof Guey-Yueh Shi for administrative support in establishing the animal surgery facility.

AUTHOR CONTRIBUTIONS

Conception and design: PL, LC, YY, HW, MJ
Analysis and interpretation: PL, YW, GL, YS, AS
Data collection: PL, YW, GL, YS, AS, MJ
Writing the article: PL, MJ
Critical revision of the article: PL, YY, HW, MJ
Final approval of the article: PL, YW, GL, YS, AS, LC, YY, HW, MJ
Statistical analysis: PL, YW, GL, YS, AS, MJ
Obtained funding: PL, LC, HW, MJ
Overall responsibility: MJ

REFERENCES

1. Nordon IM, Hinchliffe RJ, Loftus IM, Thompson MM. Pathophysiology and epidemiology of abdominal aortic aneurysms. Nat Rev Cardiol 2011;8:92-102.
2. Longo GM, Xiong W, Greiner TC, Zhao Y, Fiotti N, Baxter BT. Matrix metalloproteinases 2 and 9 work in concert to produce aortic aneurysms. J Clin Invest 2002;110:625-32.
3. Verhoeven EL, Kapma MR, Groen H, Tielliu IF, Zeebregts CJ, Bekkema F, et al. Mortality of ruptured abdominal aortic aneurysm treated with open or endovascular repair. J Vasc Surg 2008;48:1396-400.
4. Blankensteijn JD, de Jong SE, Prinssen M, van der Ham AC, Buth J, van Sterkenburg SM, et al. Two-year outcomes after conventional or endovascular repair of abdominal aortic aneurysms. N Engl J Med 2005;352:2398-405.
5. Heller JA, Weinberg A, Arons R, Krishnasastry KV, Lyon RT, Deitch JS, et al. Two decades of abdominal aortic aneurysm repair: have we made any progress? J Vasc Surg 2000;32:1091-100.
6. Wassef M, Upchurch GR Jr, Kuivaniemi H, Thompson RW, Tilson MD 3rd. Challenges and opportunities in abdominal aortic aneurysm research. J Vasc Surg 2007;45:192-8.
7. Golledge J, Muller J, Daugherty A, Norman P. Abdominal aortic aneurysm: pathogenesis and implications for management. Arterioscler Thromb Vasc Biol 2006;26:2605-13.
8. Vorp DA, Vande Geest JP. Biomechanical determinants of abdominal aortic aneurysm rupture. Arterioscler Thromb Vasc Biol 2005;25:1558-66.
9. Thompson RW, Geraghty PJ, Lee JK. Abdominal aortic aneurysms: basic mechanisms and clinical implications. Curr Probl Surg 2002;39:110-230.
10. Trollope A, Moxon JV, Moran CS, Golledge J. Animal models of abdominal aortic aneurysm and their role in furthering management of human disease. Cardiovasc Pathol 2011;20:114-23.
11. Smith AC, Swindle MM. Preparation of swine for the laboratory. ILAR J 2006;47:358-63.
12. Vollmar JF, Paes E, Pauschinger P, Henze E, Friesch A. Aortic aneurysms as late sequelae of above-knee amputation. Lancet 1989;2:834-5.
13. Nakahashi TK, Hoshina K, Tsao PS, Sho E, Sho M, Karwowski JK, et al. Flow loading induces macrophage antioxidative gene expression in experimental aneurysms. Arterioscler Thromb Vasc Biol 2002;22:2017-22.
14. Guzman RJ, Abe K, Zarins CK. Flow-induced arterial enlargement is inhibited by suppression of nitric oxide synthase activity in vivo. Surgery 1997;122:273-9; discussion: 279-80.

15. Humphrey JD, Taylor CA. Intracranial and abdominal aortic aneurysms: similarities, differences, and need for a new class of computational models. Annu Rev Biomed Eng 2008;10:221-46.
16. Cheng C, Tempel D, van Haperen R, van der Baan A, Grosveld F, Daemen MJ, et al. Atherosclerotic lesion size and vulnerability are determined by patterns of fluid shear stress. Circulation 2006;113: 2744-53.
17. Lin JH, Chu RM, Yang PC, Weng CN, Lin PH, Liu SK, et al. Influence of age on the electrocardiographic waves in Taiwanese Lan-Yu miniature pigs. Contemp Top Lab Anim Sci 1999;38:36-41.
18. Dua MM, Dalman RL. Hemodynamic influences on abdominal aortic aneurysm disease: application of biomechanics to aneurysm pathophysiology. Vasc Pharmacol 2010;53:11-21.
19. Dobrin PB. Poststenotic dilatation. Surg Gynecol Obstet 1991;172: 503-8.
20. Beldi G, Bosshard A, Hess OM, Althaus U, Walpoth BH. Transit time flow measurement: experimental validation and comparison of three different systems. Ann Thorac Surg 2000;70:212-7.
21. Aleksic M, Heckenkamp J, Gawenda M, Brunkwall J. Pulsatility index determination by flowmeter measurement: a new indicator for vascular resistance? Eur Surg Res 2004;36:345-9.
22. Silvilairat S, Cetta F, Biliciler-Denktas G, Ammash NM, Cabalka AK, Hagler DJ, et al. Abdominal aortic pulsed wave Doppler patterns reliably reflect clinical severity in patients with coarctation of the aorta. Congenit Heart Dis 2008;3:422-30.
23. Pfammatter JP, Berdat P, Carrel T. Impaired poststenotic aortic pulsatility after hemodynamically ideal coarctation repair in children. Pediatr Cardiol 2004;25:495-9.
24. Hu JJ, Ambrus A, Fossum TW, Miller MW, Humphrey JD, Wilson E. Time courses of growth and remodeling of porcine aortic media during hypertension: a quantitative immunohistochemical examination. J Histochem Cytochem 2008;56:359-70.
25. Davis V, Persidskaia R, Baca-Regen L, Itoh Y, Nagase H, Persidsky Y, et al. Matrix metalloproteinase-2 production and its binding to the matrix are increased in abdominal aortic aneurysms. Arterioscler Thromb Vasc Biol 1998;18:1625-33.
26. Lopez-Candales A, Holmes DR, Liao S, Scott MJ, Wickline SA, Thompson RW. Decreased vascular smooth muscle cell density in medial degeneration of human abdominal aortic aneurysms. Am J Pathol 1997;150:993-1007.
27. Hoshina K, Sho E, Sho M, Nakahashi TK, Dalman RL. Wall shear stress and strain modulate experimental aneurysm cellularity. J Vasc Surg 2003;37:1067-74.
28. Huang J, Davis EC, Chapman SL, Budatha M, Marmorstein LY, Word RA, et al. Fibulin-4 deficiency results in ascending aortic aneurysms: a potential link between abnormal smooth muscle cell phenotype and aneurysm progression. Circ Res 2010;106:583-92.
29. Shen D, Li J, Lepore JJ, Anderson TJ, Sinha S, Lin AY, et al. Aortic aneurysm generation in mice with targeted deletion of integrin-linked kinase in vascular smooth muscle cells. Circ Res 2011;109:616-28.
30. Hsiai TK. Mechanosignal transduction coupling between endothelial and smooth muscle cells: role of hemodynamic forces. Am J Physiol Cell Physiol 2008;294:C659-61.
31. Finol EA, Amon CH. Flow-induced wall shear stress in abdominal aortic aneurysms: part II—pulsatile flow hemodynamics. Comput Methods Biomech Biomed Eng 2002;5:319-28.
32. Dalman RL. Oxidative stress and abdominal aneurysms: how aortic hemodynamic conditions may influence AAA disease. Cardiovasc Surg 2003;11:417-9.
33. Greve JM, Les AS, Tang BT, Draney Blomme MT, Wilson NM, Dalman RL, et al. Allometric scaling of wall shear stress from mice to humans: quantification using cine phase-contrast MRI and computational fluid dynamics. Am J Physiol Heart Circ Physiol 2006;291: H1700-8.
34. Molacek J, Treska V, Kobr J, Certik B, Skalicky T, Kuntscher V, et al. Optimization of the model of abdominal aortic aneurysm—experiment in an animal model. J Vasc Res 2009;46:1-5.
35. Finol EA, Keyhani K, Amon CH. The effect of asymmetry in abdominal aortic aneurysms under physiologically realistic pulsatile flow conditions. J Biomech Eng 2003;125:207-17.

Submitted May 2, 2012; accepted Aug 16, 2012.

Additional material for this article may be found online at www.jvascsurg.org.

APPENDIX (online only)

METHODS

Gelatin zymography. Gelatinases were extracted according to a previously published method.[1] Briefly, tissue chunks of the distal abdominal aorta (AA) segment were powdered in liquid nitrogen. Samples were homogenized and extracted twice in TNC buffer (50 mmol/L Tris base, 150 mmol/L NaCl, 10 mmol/L $CaCl_2$, 0.05% Brij 35, and 0.02% NaN_3), twice in TNC buffer containing 2% dimethyl sulfoxide, and once in TNC buffer containing 10 M urea. Tissue homogenates (30 μg of protein) were separated with sodium dodecyl sulfate-polyacrylamide gel electrophoresis containing 0.1% gelatin under nonreducing condition at 4°C. Gels were renatured, developed for 16 hours at 37 °C, stained with Coomassie blue, and destained until clear bands were detected. Gelatinolytic activity was analyzed with densitometry.

RESULTS

Structural changes in the suprarenal and distal AA segments during AAA formation. No significant change in elastic lamella density was detected in the suprarenal and proximal AA segments (Appendix Fig, *A* and *B,* online only). No changes in collagen fiber density and distribution were detected in the suprarenal and proximal AA segments throughout the 12-week postcoarctation period compared with sham control (Appendix Fig, *C* and *D,* online only). The nuclear density in the media did not change markedly in the suprarenal and proximal AA segments, with the exception of the proximal AA at 4 weeks postcoarctation (Appendix Fig, *E* and *F,* online only).

REFERENCE

1. Davis V, Persidskaia R, Baca-Regen L, Itoh Y, Nagase H, Persidsky Y, et al. Matrix metalloproteinase-2 production and its binding to the matrix are increased in abdominal aortic aneurysms. Arterioscler Thromb Vasc Biol 1998;18:1625-33.

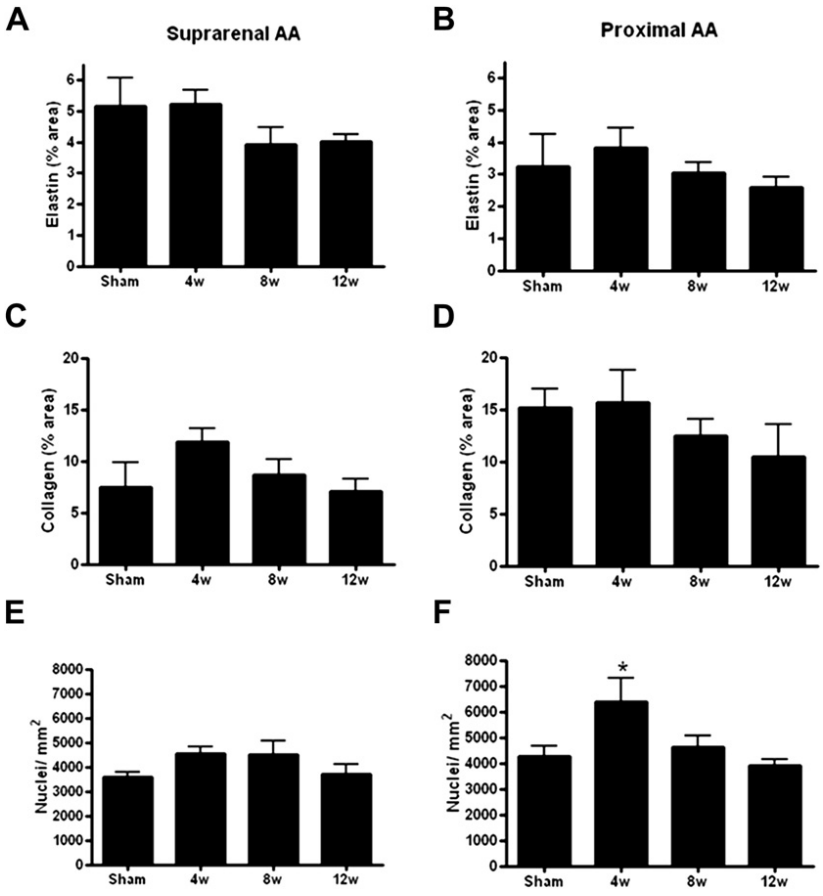

Appendix Fig (online only). Structural features of the suprarenal and proximal abdominal aortic segments following coarctation. Cross sections of the suprarenal **(A, C, E)** and proximal abdominal aorta (*AA*) **(B, D, F)** segments were stained for elastic fibers **(A** and **B),** collagen fibers **(C** and **D),** and smooth muscle-specific α-actin (SMA) and nucleus **(E** and **F)**. The percent area of elastic fibers and collagen fibers was analyzed in four sections with four fields per section as described in the Methods. Results were presented as mean ± standard error of the mean (elastic staining, n = 3∼9; collagen staining, n = 3∼4). The SMA-positive area was used to define the media, and the number of nuclei in five or six fields of the media was counted. Nuclear density was calculated and presented as mean ± standard error of the mean (n = 3∼8).